ORIGINAL RESEARCH

High-energy ball milling technique for ZnO nanoparticles as antibacterial material

Numan Salah[1]
Sami S Habib[1]
Zishan H Khan[1]
Adnan Memic[1]
Ameer Azam[1]
Esam Alarfaj[2]
Nabeel Zahed[3]
Salim Al-Hamedi[3]

[1]Center of Nanotechnology, King Abdulaziz University, Jeddah; [2]Department of Physics, Umm Al Qura University, Makkah Al Mukarramah; [3]Department of Biological Science, King Abdulaziz University, Jeddah, Saudi Arabia

Abstract: Nanoparticles of zinc oxide (ZnO) are increasingly recognized for their utility in biological applications. In this study, the high-energy ball milling (HEBM) technique was used to produce nanoparticles of ZnO from its microcrystalline powder. Four samples were ball milled for 2, 10, 20, and 50 hours, respectively. The structural and optical modifications induced in the 'as synthesized' nanomaterials were determined by X-ray diffraction (XRD), scanning electron microscopy (SEM), transmission electron microscope (TEM), and photoluminescence emission spectra (PL). SEM and TEM results show a gradual decrease in particle size from around 600 to ~30 nm, with increased milling time. The initial microstructures had random shapes, while the final shape became quite spherical. XRD analysis showed ZnO in a hexagonal structure, broadening in the diffracted peaks and going from larger to smaller particles along with a relaxation in the lattice constant c. The value of c was found to increase from 5.204 to 5.217 Å with a decrease in particle size (600 to ~30 nm). PL result showed a new band at around 365 nm, whose intensity is found to increase as the particles size decreases. These remarkable structural and optical modifications induced in ZnO nanoparticles might prove useful for various applications. The increase in c value is an important factor for increasing the antibacterial effects of ZnO, suggesting that the HEBM technique is quite suitable for producing these nanoparticles for this purpose.

Keywords: ZnO nanoparticles, antibacterial, HEBM, SEM, XRD, photoluminescence

Introduction

Nanoparticles have attracted much attention due to their distinct characteristics, which are unavailable in conventional macroscopic materials. For example, the reactions of nanoparticles with other materials can be more efficient due to their high surface-to-volume ratios, in addition to the high percentage of atoms at the grain boundaries. Some studies have found biomedical applications for nanoparticles mainly as antibacterial material,[1] cell imaging,[2] drug delivery, and cancer therapy.[3]

Zinc oxide (ZnO) is a potential material for many applications such as gas sensors, short-wavelength light-emitting devices, blue lasers, transparent conductive coatings for flat panels, solar cells, surface acoustic wave devices, and so on.[4–6] In addition to its novel physical properties,[7–9] it belongs to a group of metal oxides that are characterized by their photocatalytic and photo-oxidizing ability against chemical and biological species.[10] ZnO is, therefore, recognized for its utility in biological applications as an antibacterial material.[11–14]

Efforts have been focused on the synthesis and modification of ZnO particles for different applications. Different forms of ZnO nanostructures such as nanowires,

Correspondence: Numan Salah
Center of Nanotechnology, King Abdulaziz University, Jeddah-21589, Saudi Arabia
Tel +966 26951595
Fax +966 26951449
Email nsalah@kau.edu.sa

863

nanotubes, nanorods, and nanotetrapods were fabricated using different methods including thermal evaporation,[8] vapor phase transport (VTP),[15] metal-organic vapor-phase epitaxy (MOVPE) CVD,[16] dip coating,[17] hydrothermal route,[18] electrochemical deposition[19] and aqueous thermal decomposition.[20] Although the ZnO nanostructures fabricated using these methods have a high-purity and high-crystalline structure, the growth temperature is too high to make them compatible with low-temperature endurance substrates such as glass. The low production rate is also another problem. Therefore, we need a low-temperature, large-scale, and simple synthetic process for the synthesis of ZnO nanoparticles.

Recently, mechanical milling has proved to be an effective and simple technique without involving high temperature treatment for the production of nanocrystalline powders, with the possibility of obtaining large quantities of materials with modified properties.[21–25] In this technique, starting powder particles are trapped between highly kinetic colliding balls and the inner surface of the vial, which causes repeated deformation, rewelding, and fragmentation of premixed powders resulting in the formation of fine, dispersed particles in the grain-refined matrix. During the milling operation, two essential processes affect the particle characteristics.[22] First, the cold welding process leads to an increase in average particle size of the composite. The second, fragmentation, process causes the breaking up of composite particles. Steady-state equilibrium is attained when a balance is achieved between these processes after a certain period of milling.

The major use of the conventional ball milling is to fracture the particles and to reduce the size, which is different from the newly established high energy ball milling (HEBM) method. In this new method a magnet is placed close to the cell to apply a strong magnetic pulling force on the magnetic milling balls, and therefore the impact energy is much higher than the conventional ball milling energy. In addition, different milling actions and intensities can be achieved by adjusting the cell rotation rate and the magnet position. Four cells can be run at the same time to produce large quantities of materials. The cell rotates at a controlled rate with a high speed of 300 rpm. Moreover, in the HEBM a longer milling time is generally required to activate and complete the structural and chemical changes, crucial for the production of the desired characteristics. Using HEBM, many new meta-stable materials have been successfully produced. These new meta-stable materials cannot be synthesized using thermal equilibrium processes available

over the past several decades,[26] such as amorphization of ZrNi alloys under a dynamic equilibrium between the mechanical driven disordering or amorphization process and thermal reordering process,[27] mechanical alloying of nanocrystalline compounds, nanoparticle-reinforced metal nanocomposite,[28] or nanoporous materials.[29] Using controlled reactive ball milling, the researchers have produced nanosized particles of metal oxides,[30] nitrides,[31] hydrides,[32] and carbides[33] at room temperature. Therefore, in view of the importance of the HEBM method in nanostructures synthesis and the modification of their properties, we applied this technique in ZnO nanoparticles synthesis. Micro-structural (X-ray diffraction [XRD]), morphological (scanning electron microscope [SEM] and transmission electron microscope [TEM]), and optical studies (photoluminescence emission spectra [PL]) on the 'as-produced' ZnO nanoparticles were investigated in this research. These studies have demonstrated remarkable results on this material, which might be useful for various applications such as an antibacterial material.

Materials and methods

Commercially available ZnO powder (size $\approx$ 0.6–1 μm, purity 99.9%, Loba, Chemi, Pvt. Ltd, India) was milled in steel cells (250 mL) using hardened steel balls (diameter 15 mm, weight 32 gm) in ambient atmosphere for different times ranging from 2 to 50 hours. The mechanical milling was performed in a horizontal oscillatory mill (Retsch, PM 400) operating at 25 Hz. The mixture ratio of steel balls and ZnO powders was around 15:1 by weight percent. The milled materials were used directly with no added milling media. Five balls were kept in each cell along with 10 g of the sample powder. Two parallel cells were used in this experiment (the total weight for the sample powder was 20 g). The as synthesized materials were characterized by X-ray diffraction, using an Ultima-IV (Rigaku, Japan) diffractometer with Cu Kα radiation, while the morphology of the powders was analyzed using a field emission scanning electron microscope (FESEM), JSM-7500 F (JEOL-Japan) operated at 10 kV and also by a TEM. TEM images were obtained on a JEOL JEM 2000EX, operated at 200 kV. Photoluminescence emission spectra (PL) were recorded at room temperature using a fluorescence sectrofluorophotometer, model RF-5301 PC, Shimadzu, Japan. For PL measurements, equal quantities of the nanomaterials was dispersed in ethanol (5 mg in 5 mL) and then used for recording the spectra.

Results

X-rays diffraction

The XRD patterns for the ZnO powders as purchased and after different milling times are shown in Figure 1. The diffractograms display the reflection lines of hexagonal ZnO (space group: P 63 mc).[34] It is clear from Figure 1 that with increasing milling time, the corresponding peaks become broader and less intense. This might be due to the reduction in the particle size.[35] The XRD analysis shows a significant modification in the lattice constant c. The value of c is found to increase from 5.204 to 5.217 Å, while going from bigger particles to smaller ones (Table 1). Meanwhile no systemic change was observed in the values of lattice constants, a and b. The value of c was found to increase exponentially as a function of mailing time (particle size). This behavior is illustrated in Figure 2. The average particle size of the sample milled for 50 hours was also calculated using the Debye–Scherrer formula and found to be around 22 nm.

Scanning and transmission electron microscopes

Figure 3(A1) shows the SEM image of the starting ZnO sample without HEBM. This sample contains particles of different sizes/shapes (covering the range 0.1–0.6 μm) and more than 80% of these particles are large (close to 0.6 μm). SEM images of the ZnO samples milled for 2, 10, 20, and 50 hours are presented in Figure 3E1, C1, D1, and E1, respectively. The images of the samples milled for 2 and 10 hours, show particles of smaller size, but unsystematic shapes (Figure 3B1 and C1, respectively), whereas the samples milled for 20 hours show smaller and almost spherical shaped nanoparticles (Figure 3D1). The sample
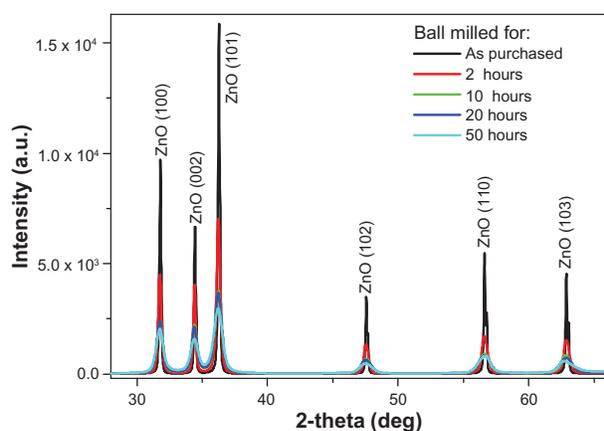
Table 1 Lattice constants a, b, and c for ZnO nanoparticles before and after ball milling for different times

Milling time (h)	a (Å)	b (Å)	c (Å)
0	3.248190	3.248190	5.204515
2	3.255058	3.255058	5.208783
10	3.251544	3.251544	5.212723
20	3.253111	3.253111	5.214094
50	3.250677	3.250677	5.216862

milled for 50 hours contains very fine nanoparticles with spherical shapes and almost equal sizes ~30 nm (Figure 3E1). The average particle size estimated from SEM images is plotted as a function of milling time and shown in Figure 4. This figure shows an exponentially decreasing behavior with increased milling time.

TEM images for the ZnO samples before and after milling (Figure 5A2–E2) were also obtained. These images display similar trends to those observed by SEM images (Figure 3 A1–E1). The sample milled for 50 hours (Figure 5E2) contains ultrafine particles of sizes in the range 20–30 nm, which are close to those observed by SEM (Figure 3E1). These sizes are also in agreement with that obtained by the Debye–Scherrer formula (~22 nm). This is a remarkable result, achieved with this simple method for producing ultrafine spherical nanoparticles of ZnO on a large scale, which might be useful for various applications.

Optical properties

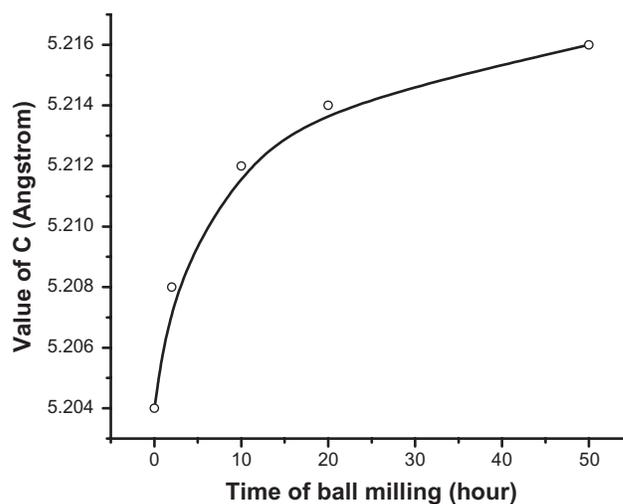PL of ZnO nanocrystalline samples prepared by the HEBM technique at different times are shown in Figure 6.

Figure 1 X-ray diffracted peaks of ZnO nanoparticles before and after ball milled for different times.

Figure 2 The value of the lattice constant c as a function of milling time.
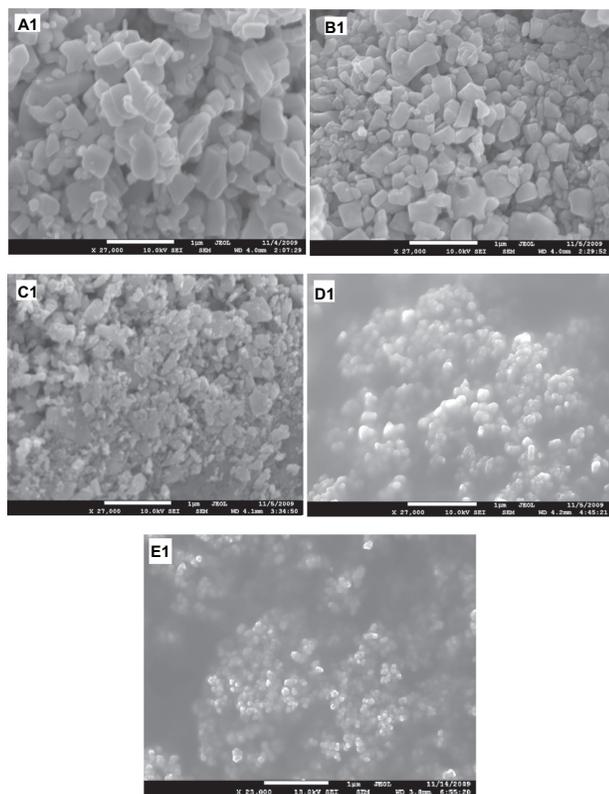
Figure 3 Scanning electron microscope images of ZnO samples before and after milling: (**A1**) as purchased. (**B1**, **C1**, **D1**, and **E1**) for the samples ball milled for 2, 10, 20, and 50 hours respectively.

Figure 5 Transmission electron microscope images of ZnO samples before and after milling; (**A2**) as purchased (**B2**, **C2**, **D2** and **E2**) for the samples ball milled for 2, 10, 20, and 50 hours respectively.

The samples were excited by 325 nm. The micro size material (before milling) shows a single intense emission band at 384 nm (Figure 6, curve a) along with a broader one covering the range of 420–600 nm, with a lesser intensity. The latter has its maximum intensity at around 440 nm. After milling for 2 hours, the band at 384 nm was found to decrease as a new band emerged at around 365 nm (Figure 6). The intensity
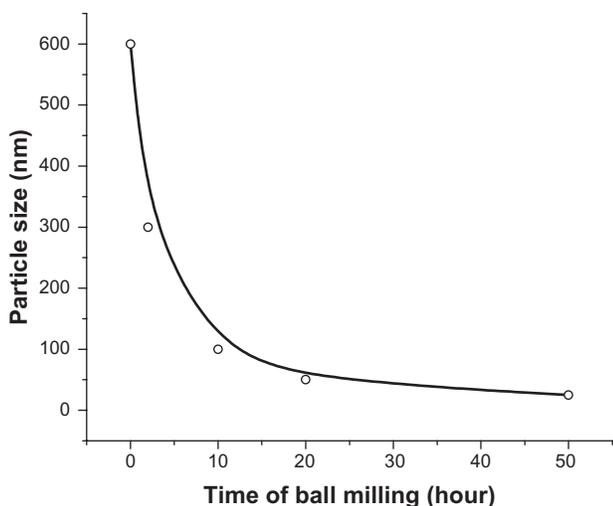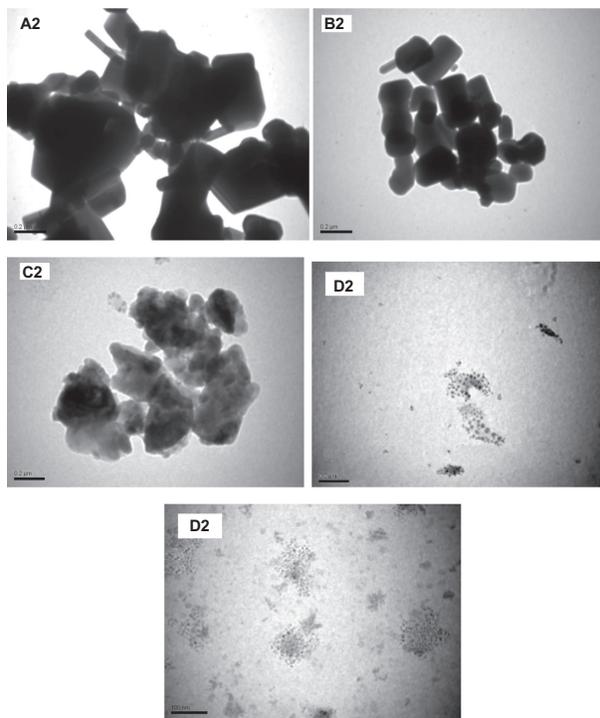
of this new band increased with decreasing particle size. It is plotted as a function of milling time and found to have a linear relationship, as shown in Figure 7 (curve a). This relationship matched the theoretical function: $y = 0.3x + 1.5$, whose curve is plotted and shown in Figure 7 (curve b). The broad band with maximum intensity at 440 nm was found to shift to the higher wavelength region and become more prominent at the smallest particle size (30 nm). This shift in
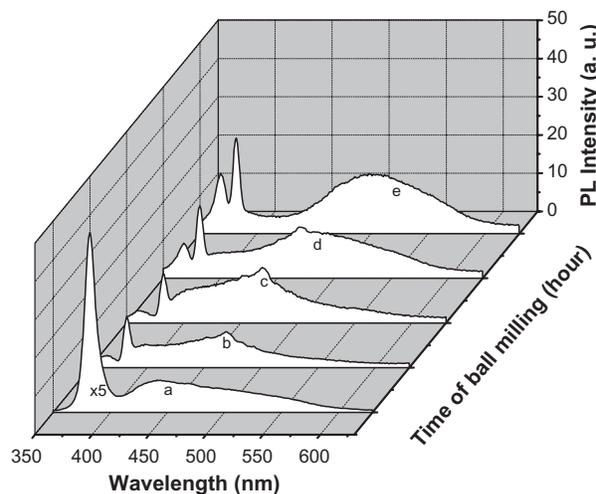

Figure 4 Particle size as a function of milling time.

Figure 6 Photoluminescence emission spectra of ZnO nanocrystalline samples prepared by ball milling at different times. The excitation wavelength is 325 nm.
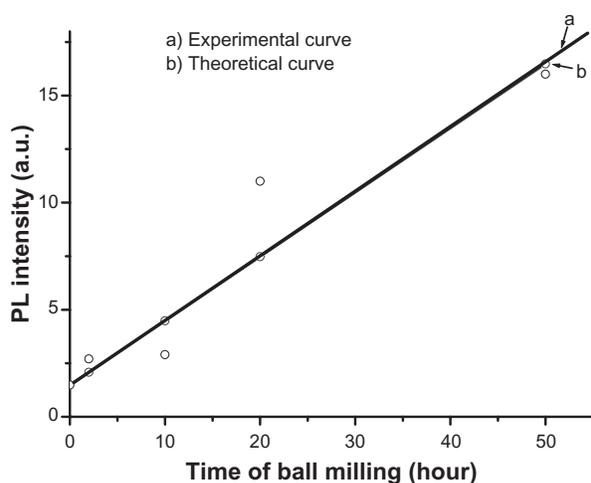**Abbreviation:** PL, photoluminescence.

Figure 7 Photoluminescence intensity of the peak at 365 nm as a function of milling time (size of ZnO nanoparticles): (a) experimental curve, (b) theoretical curve.
Abbreviation: PL, photoluminescence.

band position resulted in a change in color of the samples. The initial color of the sample was white, but the color of the final product became green. The band at 384 nm is the UV near-band edge emission.[36,37] The other broad band, peaking at 440 nm, was attributed to the deep defect levels of oxygen vacancies or interstitial zinc ions.[38–41] Vendhausen et al[42] assigned the green emission at 510 nm to the transition between the photoexcited holes and singly ionized oxygen vacancy.

Discussion

The present study demonstrates remarkable experimental results on ZnO material. A number of workers have produced this material using the same technique,[21–25] but some of the modifications observed in this study have not been reported earlier. These include the final shapes of the nanoparticles, which became quite spherical (Figure 3E1). The other remarkable result is the lattice relaxation in z direction by means of a significant increase in value of the lattice constant c (Table 1). It is well known that milling is a process involving complex mechanical forces, therefore, it is expected that these forces act equally on all sides of the particles due to the long milling time (50 hours), resulting in the formation of quite spherical particles. In other words, a balance between the striking force causing fraction of the particles and the material resistance is achieved at particle size around 30 nm. Obtaining nanoparticles of ZnO in this size (30 nm) is a remarkable result, maybe due to the use of the high-energy ball milling technique. Other investigators have reported[41,43] that when the particles become small enough (typically hundreds of nm), further refinement cannot be observed due to equilibration of cold welding and fracturing. In these cases, this might be due

to the use of the conventional ball milling technique, which is different from the high-energy ball milling used in our study. It has been reported that the impact energy of HEBM is typically 1000 times higher than the conventional ball milling energy.[43] The major use of the conventional ball milling is to fracture the particles and to reduce the size, while in high energy ball milling, a longer milling time can be achieved, which can help to activate and complete the structural changes and chemical reactions which are crucial to produce the desired structural changes or chemical reactions. HEBM can perform most of the work normally performed by conventional ball milling. Therefore, conventional ball milling system cannot be used directly to conduct any HEBM work and specially designed ball mills with a higher milling energy are preferred for HEBM.[43]

Lattice relaxation of ZnO in z direction observed in our study has also been reported by a number of workers. For example, Bao et al[44] reported on the observation of slightly higher c values for ZnO thin films prepared on quartz glass substrates by sol–gel method. Hideyuki Maki et al[45] claimed that a lattice relaxation occurs along the z-axis, which is due to the polarity occurring in that direction. In the present study, the increase in value of the lattice constant c might be due to the occurrence of strain in the nanoparticles as a result of loss of oxygen ions. It is quite possible that the continuous loss of oxygen ions during the milling (as could be seen from the PL results presented in Figure 6) might have induced such strain in the lattice of ZnO. Our view in this case is supported by the observation of other investigators such as Sun et al,[46] who have observed a linear decrease in value of the lattice constant c of ZnO with increasing oxygen pressure during the growth of ZnO film. The present result clearly shows a loss in oxygen ions as revealed from the PL spectrum; in this case it might be possible that the uppermost zinc ions were relaxed toward the outside of the surface by a significant value of the c lattice constant during the loss of oxygen ions. Moreover, there might also be modifications in the luminescent centers inside the host of the nanoparticles, resulting in a huge shift in the emissions at 440 nm towards the higher wavelengths. However, emergence of a new band at around 365 nm is questionable. This band has a shorter wavelength than that of the band gap of ZnO (384 nm). This band cannot be assigned to any impurity inside the host (such as iron as contamination from the steel balls), because it shows emission above the band gap. Hence, we might speculate that there might be a new phase of ZnO, induced with a wider band gap due to the high temperature generated in the medium as a result of using HEBM. Ultrafine nanoparticles smaller than 30 nm of ZnO might also be present, whose energy band gap

is higher than the initial microstructures. However, this needs to be investigated using other techniques such as differential thermal analysis (DTA) or differential scanning calorimetry (DSC) to identify the origin of the 365 nm band.

ZnO nanoparticles with modified properties might have a potential application as an efficient antibacterial material, since a number of researchers have reported that ZnO has an antibacterial effect.[11–14] This effect is increased with the increase of c value as revealed by Yamamoto et al.[11] This slight change in the crystal structure of ZnO due to the increase in c value has a great effect on the amount of H_2O_2 generated from the surface of ZnO crystals, which in turn is effective for the inhibition of bacterial growth.[11] Moreover, this material was reported to show antibacterial activity in the neutral region (pH 7) without the presence of light. Therefore these ZnO nanoparticles, obtained using HEBM might be ideal for antibacterial applications at different places/environments.

Conclusion

The structural and optical modifications induced in ZnO powder using the HEBM technique were investigated. These include formation of quite spherical and very fine nanoparticles of ZnO with almost equal sizes, lattice relaxation in the z-axis direction, deep level defects caused by oxygen loss, and emergence of a new PL band at 365 nm, which might be due to a new phase formation. These structural and optical modifications suggest that ZnO nanoparticles might have a potential application as an efficient antibacterial material. Moreover, the HEBM technique was found to be effective for producing ultrafine spherical nanoparticles of ZnO on a large scale, which might be useful for various applications.

Acknowledgment

Disclosure

The authors declare no conflicts of interest.

References

1. Puckett SD, Taylor E, Raimondo T, et al. The relationship between the nanostructure of titanium surfaces and bacterial attachment. *Biomaterials*. 2010;31:706–713.
2. Seo WS, Lee JH, Sun X, et al. FeCo/graphitic shell nanocrystals as advanced magnetic-resonance-imaging and near infrared agents. *Nat Mater*. 2006;5(12):971–976.
3. Dilnawaz F, Singh A, Mohanty C, Sahoo SK. Dual drug loaded superparamagnetic iron oxide nanoparticles for targeted cancer therapy. *Biomaterials*. 2010;3:3694–3706.
4. Chen Z, Shan Z, Cao MS, et al. Zinc oxide nanotetrapods. *Nanotechnology*. 2004;15:365.
5. Wu J, Xie CS, Bai ZK, et al. Preparation of ZnO-glass varistor from tetrapod ZnO nanopowders. *Mater Sci Eng B*. 2002;95:157–161.
6. Xu JQ, Pan QY, Shun YA, Tian ZZ. Grain size control and gas sensing properties of ZnO gas sensor. *Sensor Actuat B-Chem*. 2000;66(1–3): 277–279.
7. Lim SJ, Kwon SJ, Kim H. ZnO thin films prepared by atomic layer deposition and rf sputtering as an active layer for thin film transistor. *Thin Solid Films*. 2008;516(7):1523–1528.
8. Yousefi R, Muhamad MR, Zak AK. The effect of source temperature on morphological and optical properties of ZnO nanowires grown using a modified thermal evaporation set-up. *Curr Appl Phys*. 2011;11(3): 767–770.
9. Zhang H, Chen B, Jiang H, et al. A strategy for ZnO nanorod mediated multi-mode cancer treatment. *Biomaterials*. 2011;32(7):1906–1914.
10. Szabo T, Nemeth J, Dekany I. Zinc oxide nanoparticles incorporated in ultrathin layer silicate films and their photocatalytic properties. *Colloids Surfaces A*. 2003;230:23–35.
11. Yamamoto O, Komatsu M, Sawai J, et al. Effect of lattice constant of zinc oxide on antibacterial characteristics. *J Mater Sci-Mater M*. 2004; 15:847–851.
12. Premanathan M, Karthikeyan K, Jeyasubramanian K, et al. Selective toxicity of ZnO nanoparticles toward Gram-positive bacteria and cancer cells by apoptosis through lipid peroxidation. *Nanomedicine: Nanotechnology, Biology, and Medicine*. (In press, 2010, doi:10.1016/j. nano.2010.10.001).
13. Ma X-Y, Zhang W-D. Effects of flower-like ZnO nanowhiskers on the mechanical, thermal and antibacterial properties of waterborne polyurethane. *Polym Degrad Stabil*. 2009;94(7):1103–1109.
14. G Yamamoto O, Sawai J, Sasamoto T. Change in antibacterial characteristics with doping amount of ZnO in MgO–ZnO solid solution. *Int J Inorg Mater*. 2000;2:451–454.
15. Tang H, Ye Z, Zhu L, et al. Synthesis of radial ZnO nanostructures by a simple thermal evaporation method. *Physica E*. 2008;40(3):507–511.
16. Wang JR, Ye ZZ, Huang JY, et al. ZnMgO nanorod arrays grown by metal-organic chemical vapor deposition. *Mater Lett*. 2008;62(8–9): 1263–1266.
17. Sasani Ghamsari M, Vafaee M. Sol–gel derived zinc oxide buffer layer for use in random laser media. *Mater Lett*. 2008;62(12–13):1754–1756.
18. Shao S, Jia P, Liu SC, Bai W. Stable field emission from rose-like zinc oxide nanostructures synthesized through a hydrothermal route. *Mater Lett*. 2008;62(8–9):1200–1203.
19. Ye XY, Zhou YM, Chen J, Sun YQ, Wang ZQ, et al. Coating of ZnO nanorods with nanosized silver particles by electroless plating process. *Mater Lett*. 2008;62(4–5):666–669.
20. Lin S, Tang H, Ye Z, et al. Synthesis of vertically aligned Al-doped ZnO nanorods array with controllable Al concentration. *Mater Lett*. 2008;62(4–5):603–606.
21. Damonte LC, Mendoza Zelis LA, MariSoucase B, Fenollosa Hernandez MA. Nanoparticles of ZnO obtained by mechanical milling. *Powder Technol*. 2004;148:15–19.
22. Ozdemir I, Ahrens S, Mücklich S, Bernhard W. Nanocrystalline Al Al_2O_{3p} and SiC_p composites produced by high-energy ball milling. *J Mater Process Technol*. 2008;205:111–118.
23. Lee JS, Park K, Kang M-I, et al. ZnO nanomaterials synthesized from thermal evaporation of ball-milled ZnO powders. *J Cryst Growth*. 2003;254(3–4):423–431.
24. Damontea LC, Donderis V, Hernndez-Fenollosa MA. Trivalent dopants on ZnO semiconductor obtained by mechanical milling. *J Alloy Compd*. 2009;483:442–444.
25. Glushenkov AM, Zhang HZ, Chen Y. Reactive ball milling to produce nanocrystalline ZnO. *Mater Lett*. 2008;62(24):4047–4049.
26. Koch CC. Intermetallic matrix composites prepared by mechanical alloying – a review. *Mater Sci Eng A Struct Mater*. 1998;244:39–48.
27. Chen Y, Bibole M, Lehazif R, et al. Ball-milling-induced amorphization in NixZry compounds: A parametric study. *Phys Rev B*. 1993; 48:14–21.

28. Chen Y. Mechanically enhanced carbothermic synthesis of iron-TiN composite. *J Mater Sci Lett*. 1997;16(1):37–39.

29. Chen Y, Fitz Gerald JD, Chadderton LT, et al. Nanoporous carbon produced by ball milling. *Appl Phys Lett*. 1999;74:2782.

30. Puttaswany M, Chen Y, Jar B, et al. Investigation of combustion reactions under different milling conditions. *Mater Sci Forum*. 1999; 312–314:79–84.

31. Chen Y, Calka A, Williams JS, et al. Nitriding reactions of Ti–Al system induced by ball milling in ammonia gas. *Mater Sci Eng A Struct Mater*. 1994;187:51–55.

32. Chen Y, Williams JS. Formation of metal hydrides by mechanical alloying. *J Alloy Compd*. 1995;217:181–184.

33. Chen Y, Hwang T, Marsh M, et al. Mechanically activated carbothermic reduction of ilmenite. *Metall Mater Trans A*. 1997;28:1115–1121.

34. Raoufi Davood, Raoufi Taha. The effect of heat treatment on the physical properties of sol gel derived ZnO thin films. *Appl Surf Sci*. 2009;255:5812–5817.

35. Aruna ST, Rajam KS. Mixture of fuels approach for the solution combustion synthesis of Al_2O_3–ZrO_2 nanocomposite. *Mater Res Bull*. 2004;39:157–167.

36. Sui X, Liu Y, Shao C, Liu Y, Xu CS. Structural and photoluminescent properties of ZnO hexagonal nanoprisms synthesized by microemulsion with polyvinyl pyrrolidone served as surfactant and passivant. *Chem Phys Lett*. 2006;424(4–6):340–344.

37. Wang XB, Song C, Geng KW, et al. Photoluminescence and Raman scattering of Cu-doped ZnO films prepared by magnetron sputtering. *Appl Surf Sci*. 2007;253:6905–6909.

38. Karali T, Can N, Valberg L, et al. Optical properties and luminescence of metallic nanoclusters in ZnO:Cu. *Physica B*. 2005;363:88–95.

39. Larcheri S, Armellini C, Rocca F, et al. X-ray studies on optical and structural properties of ZnO nanostructured thin films. *Superlattice Microst*. 2006;39:267–274.

40. Glushenkov AM, Zhang HZ, Chen Y. Reactive ball milling to produce nanocrystalline ZnO. *Mater Lett*. 2008;62:4047–4049.

41. Glushenkov AM, Zhang HZ, Zou J, Lu GQ, Chen Y. Efficient production of ZnO nanowires by a ball milling and annealing method. *Nanotechnology*. 2007;18(17):175604.

42. Vendhausen K, Warren WL, Seager CH, et al. Mechanisms behind green photoluminescence in ZnO phosphor powders. *J Appl Phys*. 1996;79: 7983.

43. Chen Y, Li CP, Chen H, Chen Y. One-dimensional nanomaterials synthesized using high-energy ball milling and annealing process. *Sci Technol Adva Mater*. 2006;7(8):839–846.

44. Bao D, Gu H. Kuang A. Sol-gel-derived c-axis oriented ZnO thin films. *Thin Solid Films*. 1998;312:37–39.

45. Maki H, Ichinose N, Ohashi N, Haneda H, Tanaka J. The lattice relaxation of ZnO single crystal (0001) surface. *Surf Sci*. 2000;457(3):377–382.

46. Sun L, Cheng W, Lin F, Ma XM, Shi WZ. Changes of structure and optical energy gap induced by oxygen pressure during the deposition of ZnO films. *Physica B*. 2006;381(1–2):109–112.